

# A Rapid Trajectory Optimization and Control Framework for Resource-Constrained Applications

Deep Parikh<sup>1</sup>, Thomas L. Ahrens<sup>1</sup>, Manoranjan Majji<sup>2</sup>

**Abstract**—This paper presents a computationally efficient model predictive control formulation that uses an integral Chebyshev collocation method to enable rapid operations of autonomous agents. By posing the finite-horizon optimal control problem and recursive re-evaluation of the optimal trajectories, minimization of the L2 norms of the state and control errors are transcribed into a quadratic program. Control and state variable constraints are parameterized using Chebyshev polynomials and are accommodated in the optimal trajectory generation programs to incorporate the actuator limits and keep-out constraints. Differentiable collision detection of polytopes is leveraged for optimal collision avoidance. Results obtained from the collocation methods are benchmarked against the existing approaches on an edge computer to outline the performance improvements. Finally, collaborative control scenarios involving multi-agent space systems are considered to demonstrate the technical merits of the proposed work.

## I. INTRODUCTION

There has been a significant leap during the past few years in satellite missions relying on in-space autonomy [1]. Most of these missions employ state-of-the-art Rendezvous, Proximity Operations and Docking (RPOD) and satellite swarming technologies to enable space science, earth observation, planetary defense, satellite servicing and on-orbit life extension [2], [3], [4]. One of the earliest satellite servicing missions utilized a robotic manipulator to demonstrate the on-orbit capabilities in low Earth orbit [5], and most of the proposed missions to service and repair satellites hope to leverage manipulators to grasp the target spacecraft [6].

However, the additional degrees of freedom associated with the floating base of the robot manipulator renders the analysis of system dynamics and real-time control challenging [7]. Furthermore, if the contact and capture of the target satellite are not planned carefully, the resulting momentum transfer after the capture can cause severe stability issues [8]. Consequently, most of such missions have been considered to be at a very low Technology Readiness Level (TRL) due to limited onboard autonomy constrained by Size, Weight, and Power (SWaP) [9].

On the contrary, the recent advancements in consumer electronics and sensor technology have pushed the boundaries of autonomous in-space operations [10]. The entire process of qualification, verification, and validation of such

novel hardware components and software packages have been greatly accelerated by the ease of availability of Cube-Sat manufacturers and launch providers [11]. The new form-factor of nano-satellites has also been aptly leveraged for earth observation [12], oceanography [13] and space weather monitoring [14] applications.

The Model-Predictive-Control (MPC) framework has been extensively studied for automatic control of industrial processes [15]. Although the framework has seen limited use in aerospace vehicles due to its stringent qualification, robustness and real-time requirements [16], there is an unequivocal pursuit to overcome some of these shortcomings about the complexity and computational cost. The advancements have helped bridge the gap between computationally intensive MPC and resource-constrained computers by exploiting the control structures to accelerate and compress solver algorithms [17]. This has also motivated recent studies to assess the computational requirements of a pragmatic MPC-based RPOD algorithm with the current state-of-the-art solvers [18].

Alongside the advances in available onboard hardware, many new computationally efficient algorithms have been developed to solve optimal control problems. In particular,

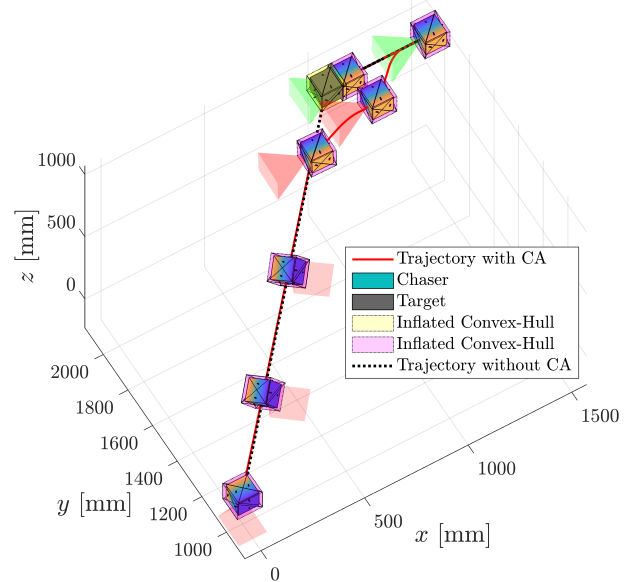


Fig. 1. Guidance algorithm for docking of TPODS with a stationary target consists of three distinct guidance modes. For each mode, TPODS is commanded to move along the optimal trajectory, which passes through the target if no collision maneuver is executed. The availability of vision measurements is depicted by a color change of the FOV cone.

\*This work is supported by the Air Force Office of Scientific Research (AFOSR), as a part of the SURI on OSAM project “Breaking the Launch Once Use Once Paradigm” (Grant No: FA9550-22-1-0093).

<sup>1</sup>PhD Student, {deep,tahrens}@tamu.edu

<sup>2</sup>Director, LASR Laboratory, Professor

Department of Aerospace Engineering, Texas A&M University, College Station, Texas, USA.

pseudospectral methods are well-known for their accuracy and robustness [19]. Recent work using integral collocation, rather than the typical derivative methods, yields enhanced precision and significant runtime speedups [20], [21]. One of these methods, known as Integral Chebyshev Collocation (ICC), has been shown to be especially accurate, and does not require the use of another (typically Legendre) interpolating polynomial [21].

To that end, this paper presents a pseudospectral-based MPC framework called MPC<sup>3</sup>: *Model Predictive Control using Chebyshev Collocation*. The main contribution of the paper, constrained quadratic programming optimization via orthogonal approximation using ICC, is introduced in Sec. II. Performance results for the proposed method are compared with existing solvers in Sec. III. Finally, Sec. IV demonstrates the effectiveness of the framework to achieve the desired objective with an application of multi-state guidance logic for a docking scenario of small satellites.

## II. MPC<sup>3</sup> FORMULATION

### A. Chebyshev Polynomial Approximation

Orthogonal polynomials play an important role in the fields of numerical analysis, approximation, and optimal control. A particularly attractive family of these orthogonal functions are the Chebyshev polynomials, which are defined over the domain  $\tau \in [-1, 1]$  as

$$T_n(\tau) = \cos(n \arccos \tau) \quad (1)$$

Any function  $f(t)$  can be mapped from the time domain  $t \in [t_0, t_f]$  to the computational domain  $\tau \in [-1, 1]$  over which the Chebyshev polynomials are defined with the linear transformation

$$\tau = \frac{2t - (t_f + t_0)}{\Delta t}, \quad \Delta t = t_f - t_0 \quad (2)$$

Thus, an approximation of the function at any point  $f(\tau)$  can be constructed as a linear combination

$$f(\tau) = \sum_{i=0}^n T_i(\tau) \alpha_i = \mathbf{T}(\tau) \boldsymbol{\alpha} \quad (3)$$

where  $\mathbf{T}(\tau) = [T_0(\tau), T_1(\tau), \dots, T_n(\tau)] \in \mathbb{R}^{1 \times (n+1)}$  is a row vector of Chebyshev polynomials evaluated at  $\tau$  and  $\boldsymbol{\alpha} = [\alpha_0, \alpha_1, \dots, \alpha_n]^\top \in \mathbb{R}^{(n+1) \times 1}$  is a column vector of unknown coefficients. Using a set of nodes  $\boldsymbol{\tau} = [\tau_0, \tau_1, \dots, \tau_n]^\top$ , the approximation of the function  $\mathbf{f}(\boldsymbol{\tau}) = [f(\tau_0), f(\tau_1), \dots, f(\tau_n)]^\top$  is formed as

$$\begin{bmatrix} f(\tau_0) \\ f(\tau_1) \\ \vdots \\ f(\tau_n) \end{bmatrix} = \begin{bmatrix} T_0(\tau_0) & T_1(\tau_0) & \cdots & T_n(\tau_0) \\ T_0(\tau_1) & T_1(\tau_1) & \cdots & T_n(\tau_1) \\ \vdots & \vdots & \ddots & \vdots \\ T_0(\tau_n) & T_1(\tau_n) & \cdots & T_n(\tau_n) \end{bmatrix} \begin{bmatrix} \alpha_0 \\ \alpha_1 \\ \vdots \\ \alpha_n \end{bmatrix} \quad (4)$$

$$\mathbf{f}(\boldsymbol{\tau}) = \mathcal{T}(\boldsymbol{\tau}) \boldsymbol{\alpha}, \quad \mathcal{T}(\boldsymbol{\tau}) \in \mathbb{R}^{(n+1) \times (n+1)} \quad (5)$$

It has been shown that the optimal set of nodes  $\boldsymbol{\tau}$  which minimize the interpolation error are the roots of the  $(n+1)$ <sup>th</sup>

order Chebyshev polynomial [22], known as the Chebyshev-Gauss (CG) nodes.

$$\tau_{k-1} = \cos\left(\frac{(k - \frac{1}{2})\pi}{n+1}\right), \quad k = [1, 2, \dots, n+1] \quad (6)$$

### B. Integral Chebyshev Collocation

Chebyshev polynomials have been the subject of much work for solving initial value problems (IVPs) and boundary value problems (BVPs). Bai and Junkins developed a procedure known as Modified Chebyshev Picard Iteration (MCPI) to converge toward a solution for IVPs and BVPs [20], [23]. More recently, Peck proposed a concise procedure known as Integral Chebyshev Collocation (ICC) [21], the method of choice for this work. This approach is described hereafter for a generic second-order dynamic system.

The ICC procedure begins by transforming the differential equation(s) to the Chebyshev domain  $\tau \in [-1, 1]$ . This is achieved simply via the chain rule by differentiating Eq. (2) with respect to  $\tau$ ,

$$\ddot{x}(t) = \frac{d^2x}{dt^2} = \frac{d^2x}{d\tau^2} \frac{d\tau^2}{dt^2} = x''(\tau) \left(\frac{2}{\Delta t}\right)^2 \quad (7)$$

$$x''(\tau) = \left(\frac{\Delta t}{2}\right)^2 \ddot{x}(t) \quad (8)$$

The first derivative and state are then transformed as

$$x'(\tau) = \left(\frac{\Delta t}{2}\right) \dot{x}(t) \quad (9)$$

$$x(\tau) = x(t) \quad (10)$$

Similarly, the initial conditions  $\dot{x}_0$  and  $x_0$  are cast to the computational domain as

$$x'(-1) = \left(\frac{\Delta t}{2}\right) \dot{x}_0, \quad x(-1) = x_0 \quad (11)$$

Now that the problem is represented in the Chebyshev domain, an  $n$ <sup>th</sup> order series of Chebyshev polynomials is used to represent the dynamics following Eq. (3).

$$x''(\tau) = \sum_{i=0}^n T_i(\tau) \alpha_i = \mathbf{T}(\tau) \boldsymbol{\alpha} \quad (12)$$

The derivative representation is then formed by integrating this series from the initial time (in the Chebyshev domain)  $\tau = -1$  to the current time  $\tau$ .

$$\int_{-1}^{\tau} x''(\tau) d\tau = \int_{-1}^{\tau} \mathbf{T}(\tau) \boldsymbol{\alpha} d\tau \quad (13)$$

$$x'(\tau) - x'(-1) = \left[ \int_{-1}^{\tau} \mathbf{T}(\tau) d\tau \right] \boldsymbol{\alpha} \quad (14)$$

The remaining bracketed vector integral can be taken term by term, where the integrals of the Chebyshev polynomials are given as [24], [25]

$$\int T_0(\tau) d\tau = T_1(\tau) \quad (15)$$

$$\int T_1(\tau) d\tau = \frac{1}{4} (T_2(\tau) + T_0(\tau)) \quad (16)$$

$$\int T_i(\tau) d\tau = \frac{1}{2} \left( \frac{T_{i+1}(\tau)}{i+1} - \frac{T_{i-1}(\tau)}{i-1} \right), \quad i \geq 2 \quad (17)$$

The derivative is represented as

$$x'(\tau) = \underbrace{\left[ \mathbf{T}(\tau)\tilde{\mathcal{F}} - \mathbf{v}(-1) \right]}_{\equiv \beta(\tau)} \boldsymbol{\alpha} + x'(-1) \quad (18)$$

where  $\tilde{\mathcal{F}} \in \mathbb{R}^{(n+1) \times (n+1)}$  is a square matrix composed of integration weights on the super- and sub-diagonals, and  $\mathbf{v}(-1) \in \mathbb{R}^{1 \times (n+1)}$  is the evaluated lower integration bound [21].

Following the same procedure by integrating Eq. (18) yields the state approximation,

$$x(\tau) = \underbrace{\left[ \mathbf{T}(\tau)\tilde{\mathcal{F}}^2 - \mathbf{v}(-1)\tilde{\mathcal{F}} - \mathbf{v}(-1)(\tau+1) \right]}_{\equiv \gamma(\tau)} \boldsymbol{\alpha} + x'(-1)(\tau+1) + x(-1) \quad (19)$$

Thus, the dynamics, derivative, and state are all approximated with a single set of polynomial coefficients  $\boldsymbol{\alpha}$ .

This procedure is then applied to CG nodes  $\tau$ , leading to the following vector-matrix collocation formulation, which can be written succinctly using the  $\beta$  and  $\gamma$  shorthand defined above.

$$x''(\tau) = \mathcal{T}(\tau)\boldsymbol{\alpha} \quad (20)$$

$$x'(\tau) = \beta(\tau)\boldsymbol{\alpha} + x'(-1) \quad (21)$$

$$x(\tau) = \gamma(\tau)\boldsymbol{\alpha} + x'(-1)(\tau+1) + x(-1) \quad (22)$$

Once an approximation order  $n$  is chosen,  $\mathcal{T}(\tau)$ ,  $\beta(\tau)$ , and  $\gamma(\tau)$  are all constant, and the initial conditions are simply added to the matrix-vector product. This leads to a drastic improvement in computational efficiency since these matrices need to be computed once, which can be done *a priori*. To solve a linear system, a single matrix inversion is required, while nonlinear systems require an iterative method to converge on the coefficient values.

### C. $L_2$ Minimization

The objective of a typical MPC is to solve an optimization problem at each time instance for a specified control horizon and produce a control input that minimizes the objective function [26]. Unlike traditional discrete MPC, the cost function for the linear dynamics  $\dot{\mathbf{x}}(t) = \mathbf{g}(t, \mathbf{x}, \mathbf{u})$  is given as a continuous integral from the current time  $t_0$  to some future time  $t_f$ . This is written as

$$\min J = \int_{t_0}^{t_f} (\mathbf{u}^\top \mathbf{W}_u \mathbf{u} + (\mathbf{x} - \mathbf{x}_t)^\top \mathbf{W}_x (\mathbf{x} - \mathbf{x}_t)) dt \quad (23)$$

where  $\mathbf{u} \in \mathbb{R}^m$  is the control,  $\mathbf{x}, \mathbf{x}_t \in \mathbb{R}^q$  are the instantaneous and target state, and  $\mathbf{W}_u \in \mathbb{R}^{m \times m}$  and  $\mathbf{W}_x \in \mathbb{R}^{q \times q}$  are the diagonal weight matrices for the control and states, respectively.  $\Delta t = t_f - t_0$  is now the time or prediction horizon associated with the problem.

For a generic double integrator  $\ddot{\mathbf{x}}(t) = \mathbf{u}(t)$ , the states and controls can both be represented by the unknown polynomial

coefficients  $\boldsymbol{\alpha}$ . Without loss of generality, consider a single degree of freedom system, which can be written as

$$x''(\tau) = u(\tau) = \mathbf{T}(\tau)\boldsymbol{\alpha} \quad (24)$$

$$x'(\tau) = \beta(\tau)\boldsymbol{\alpha} + x'(-1) \quad (25)$$

$$x(\tau) = \gamma(\tau)\boldsymbol{\alpha} + x'(-1)(\tau+1) + x(-1) \quad (26)$$

The problem is then converted to the Chebyshev domain as

$$\begin{aligned} \min J = \frac{\Delta t}{2} \int_{-1}^1 [ & u(\tau)W_u u(\tau) \\ & + (x(\tau) - x_t)W_x (x(\tau) - x_t) \\ & + (x'(\tau) - x'_t)W_{x'} (x'(\tau) - x'_t)] d\tau \end{aligned} \quad (27)$$

Plugging in Eqs. (24)-(26) leads to a form that includes terms with quadratic, linear, and no dependence on the coefficients  $\boldsymbol{\alpha}$ . The terms independent of the decision variable are constant, and can be removed from the minimization problem [27]. However, this leaves a form which is not easily integrable, given the Chebyshev polynomial representations.

To evaluate this integral, a Gaussian quadrature rule is used, which approximates the integral as a linear combination of quadrature weights and the integrand evaluated at specific node points [28].

$$\int_{-1}^{-1} g(\tau) d\tau \simeq \sum_{i=0}^n w_i g(\tau_i) \quad (28)$$

Using the CG nodes of Eq. (6), the weights are given as [29]

$$w_i = \frac{2}{n+1} \left[ 1 - 2 \frac{\sum_{k=1}^{[(n+1)/2]} \cos(2k\theta_i)}{4k^2 - 1} \right] \quad (29)$$

$$\theta_i = \frac{2i-1}{2(n+1)}\pi, \quad \tau_i = \cos \theta_i \quad (30)$$

Thus, the problem is finally written in the typical quadratic problem (QP) form

$$\min J = \frac{1}{2} \boldsymbol{\alpha}^\top H \boldsymbol{\alpha} + \mathbf{f}^\top \boldsymbol{\alpha} \quad (31)$$

where the symmetric, positive definite matrix  $H$  and vector  $\mathbf{f}$  are given as

$$H = \Delta t \left[ \sum_{i=0}^n w_i \left( (\mathbf{T}(\tau_i))^\top W_u \mathbf{T}(\tau_i) + (\boldsymbol{\gamma}(\tau_i))^\top W_x \boldsymbol{\gamma}(\tau_i) + (\boldsymbol{\beta}(\tau_i))^\top W_{x'} \boldsymbol{\beta}(\tau_i) \right) \right] \quad (32)$$

$$\mathbf{f} = \Delta t \left[ \sum_{i=0}^n w_i \left( W_x \boldsymbol{\gamma}(\tau_i) (x'(-1)(\tau_i+1) + x(-1) - x_t) + W_{x'} \boldsymbol{\beta}(\tau_i) (x'(-1) - x'_t) \right) \right] \quad (33)$$

TABLE I. Comparison of Discrete MPC and MPC<sup>3</sup>

	MPC	MPC <sup>3</sup>
State Equation	$\mathbf{x}_{k+1} = \mathbf{A}_d \mathbf{x}_k + \mathbf{B}_d \mathbf{u}, \mathbf{u} \in \mathbb{R}^m, \mathbf{x} \in \mathbb{R}^q$	$\dot{\mathbf{x}}(t) = \mathbf{g}(t, \mathbf{x}, \mathbf{u}), \mathbf{u} \in \mathbb{R}^m, \mathbf{x} \in \mathbb{R}^q$
Recursion	$\mathbf{y} = \mathbf{S}_x \mathbf{x}_k + \mathbf{S}_y \mathbf{u}$	$x''(\tau) = u(\tau) = \mathbf{T}(\tau)\boldsymbol{\alpha}$ $x'(\tau) = \boldsymbol{\beta}(\tau)\boldsymbol{\alpha} + x'(-1)$ $x(\tau) = \boldsymbol{\gamma}(\tau)\boldsymbol{\alpha} + x'(-1)(\tau + 1) + x(-1)$
Objective function	$\sum_{i=0}^{p-1} (\mathbf{u}_{k+i}^T \mathbf{W}_u \mathbf{u}_{k+i} + (\mathbf{y}_{k+i} - \mathbf{y}_r)^T \mathbf{W}_y (\mathbf{y}_{k+i} - \mathbf{y}_r))$	$\int_{t_0}^{t_f} (\mathbf{u}^T \mathbf{W}_u \mathbf{u} + (\mathbf{x} - \mathbf{x}_t)^T \mathbf{W}_x (\mathbf{x} - \mathbf{x}_t)) dt$
Decision Variables	$\mathbf{u}_k \in \mathbb{R}^{p \times m}$	$\boldsymbol{\alpha} \in \mathbb{R}^{(n+1) \times 1}$
# of Equality Constraints	0	$q$
# of Inequality Constraints	$2p \times q$	$4(n+1) \times q$

#### D. State and Input Constraints

For most practical applications, the control inputs are limited to a predefined threshold, which can be incorporated into the optimal control framework by the addition of a slack variable and input equality constraints. Similarly, it is often desired to restrict certain states throughout the duration of the trajectory within a specific boundary. For example, limiting approach velocity to a target can still allow for an overall aggressive position controller without any undesirable overshoot. Again, this can be achieved by the method of a slack variable and inequality constraints. Finally, equality constraints are placed on the states at the initial time to ensure the initial boundary conditions are met.

With these modifications, the quadratic program of Eq. (31) is written with equality and inequality constraints as

$$\min_{\boldsymbol{\chi}} J = \frac{1}{2} \boldsymbol{\chi}^T \mathbf{H} \boldsymbol{\chi} + \mathbf{f}^T \boldsymbol{\chi} \quad (34)$$

$$\text{s.t. } \mathbf{A}_{\text{eq}} \boldsymbol{\chi} = \mathbf{b}_{\text{eq}} \quad (35)$$

$$\mathbf{A} \boldsymbol{\chi} \leq \mathbf{b} \quad (36)$$

where

$$\boldsymbol{\chi} = \begin{bmatrix} \boldsymbol{\alpha} \\ \varepsilon \end{bmatrix} \in \mathbb{R}^{(n+2) \times 1} \quad (37)$$

$$\mathbf{H} = \begin{bmatrix} \mathbf{H} & \mathbf{0}_{n+1,1} \\ \mathbf{0}_{1,n+1} & \rho \end{bmatrix} \in \mathbb{R}^{(n+2) \times (n+2)} \quad (38)$$

$$\mathbf{A}_{\text{eq}} = \begin{bmatrix} \boldsymbol{\gamma}(-1) & \mathbf{0} \\ \boldsymbol{\beta}(-1) & \mathbf{0} \end{bmatrix} \in \mathbb{R}^{2 \times (n+2)} \quad (39)$$

$$\mathbf{b}_{\text{eq}} = \begin{bmatrix} 0 \\ 0 \end{bmatrix} \in \mathbb{R}^{2 \times 1} \quad (40)$$

$$\mathbf{A} = \begin{bmatrix} \mathcal{T}(\tau) & -V_u \\ -\mathcal{T}(\tau) & -V_u \\ -\boldsymbol{\beta}(\tau) & -V_{x'} \\ -\boldsymbol{\beta}(\tau) & -V_{x'} \end{bmatrix} \in \mathbb{R}^{4(n+1) \times (n+2)} \quad (41)$$

$$\mathbf{b} = \begin{bmatrix} u'_{\max} \\ -u'_{\min} \\ x'_{\max} - x'(-1) \\ -x'_{\min} + x'(-1) \end{bmatrix} \in \mathbb{R}^{4(n+1) \times 1} \quad (42)$$

and  $\mathbf{f}$  remains unchanged from Eq. (33). Here,  $\rho$  is the weight factor associated with the slack variable  $\varepsilon$ ,  $u'_{\max}/u'_{\min}$

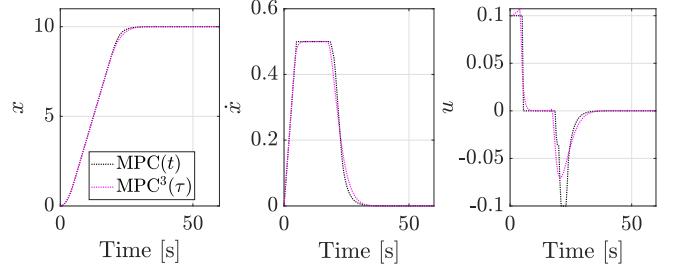


Fig. 2. Comparison of trajectories and optimal input for double integrator for  $T_s = 0.5$  s,  $p = 5$  samples, and  $n = 3$ .

and  $x'_{\max}/x'_{\min}$  are the constraints on the control and velocity converted to the Chebyshev domain, and  $V_u$  and  $V_{x'}$  are used to regulate the softness of the constraints. A comprehensive comparison of MPC<sup>3</sup> with discrete MPC along with dimensions of the optimization program is given in Table I.

### III. PERFORMANCE COMPARISON

The constrained optimization problem, now formulated in the computational domain as a quadratic program, is solved with MATLAB<sup>®</sup>'s *quadprog* using the active-set algorithm and warm-start enabled. Importantly, note that of the matrices and vectors defined in the previous section,  $\mathbf{H}$ ,  $\mathbf{A}_{\text{eq}}$ ,  $\mathbf{b}_{\text{eq}}$ , and  $\mathbf{A}$  remain unchanged, regardless of time horizon or initial conditions. Only  $\mathbf{f}$  and  $\mathbf{b}$  need to be updated at each step, resulting in an efficient formulation. The coefficients and slack variable are found by minimizing the objective function of Eq. (34), and the instantaneous control is calculated as  $u(-1) = \mathbf{T}(-1)\boldsymbol{\alpha}$ . ICC, or any other integrator, can then be used to propagate the true dynamics until reaching the next control input time.

A comparison of the optimal trajectory solutions for a double integrator system obtained via a conventional MPC and MPC<sup>3</sup> is presented in Fig. 2. Although both trajectories are very close to one another, it is important to note that both formulations do not have the same weighing factors  $\mathbf{W}_u$  and  $\mathbf{W}_x$ , and turning of these parameters is often required to ensure both solutions are identical.

#### A. Variation with State Dimension

To establish the computational gains of the proposed formulation, extensive simulation studies have been conducted

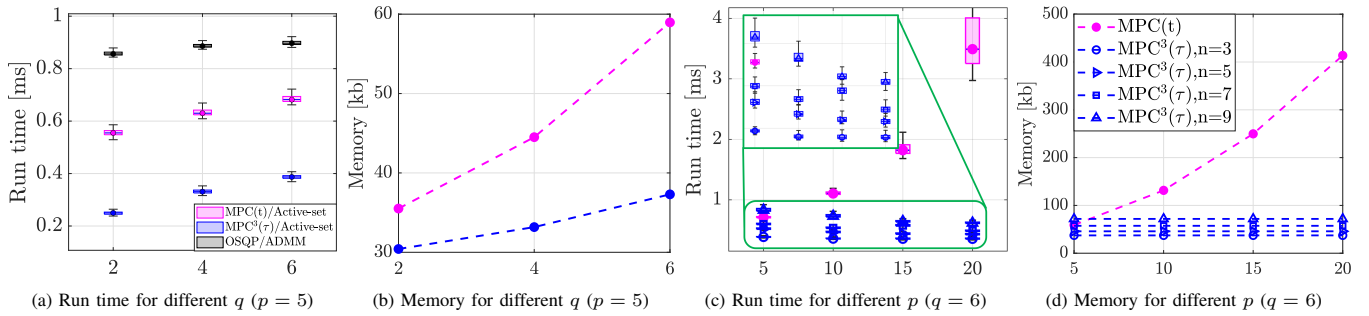


Fig. 3. Computational performance of MPC<sup>3</sup> for different state dimensions and control horizon. **Generated on a computer** with 11<sup>th</sup> Gen Intel® Core™ i5-1135G7 @ 2.40GHz, 16 GB RAM, for running a MATLAB® script. MATLAB® interface for OSQP is used to integrate OSQP [30].

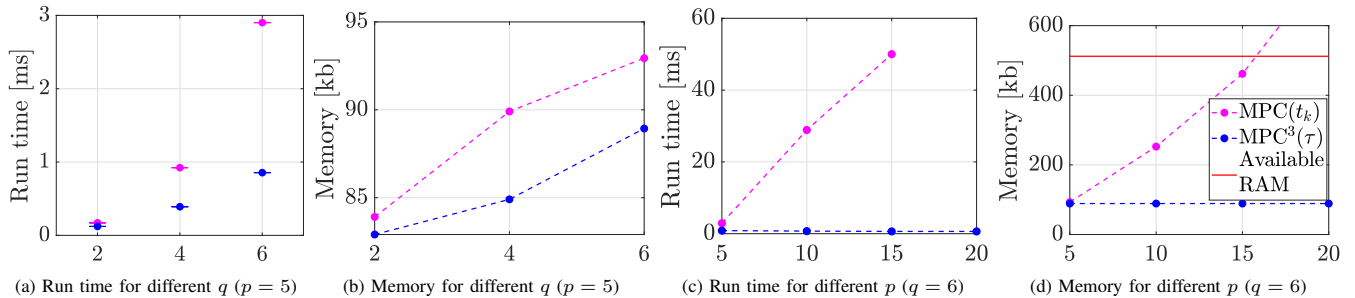


Fig. 4. Computational performance of MPC<sup>3</sup> for different state dimensions and control horizon, with fixed  $n = 3$ . **Generated on Teensy 4.1 development board**, for running a single iteration of optimization routine, built and deployed from a MATLAB® script.

and their results are presented in Fig. 3. For the first analysis, the control horizon has been kept fixed at  $p = 5$  samples and the dimension of the state  $q$  has been varied. The run time and memory requirement of a single iteration of the optimization is recorded and the comparison of MPC<sup>3</sup> with various solvers is presented in Figs. 3a and 3b. Another benefit of this MPC<sup>3</sup> formulation is that previous solutions can be used to hot start the current iteration. In particular, if the time between control inputs is relatively small and the trajectory remains relatively similar on this scale (as is expected with MPC), the previous  $\chi$  can be used as an initial guess for the current coefficients and slack variable, significantly reducing the QP runtime.

### B. Variation with Control Horizon

Further, the state dimension  $q = 6$  has been kept unchanged and the control horizon has been varied from  $p = 5$  to  $p = 20$  with an increment of 5. The results presented in Figs. 3c and 3d particularly underscore the benefits of MPC<sup>3</sup>. Since the ICC solution is global over the time horizon of interest, the runtime or memory requirements of MPC<sup>3</sup> formulation do not increase with a larger time horizon. While a larger approximation order  $n$  may be necessary to capture the greater dynamic range over this time horizon, a small increase in  $n$  is sufficient for these changes, which is shown to only marginally increase runtime.

### C. Performance Comparison on an Edge Computer

The similar analysis is also carried out for Teensy 4.1<sup>1</sup> development board to qualify the computational benefits of

the proposed framework on an embedded hardware. The MATLAB® scripts used for the earlier analysis have been built and deployed on the Teensy board using automatic code generation. The results of this exercise are presented in Figure 4, follows a similar trend of run time and memory usage for various state dimensions and control horizon. Most importantly, as the control horizon increases, the RAM usage crosses the available on-board RAM of 512 kb and the conventional MPC could no longer be implemented on the hardware. However, as mentioned earlier, the resource utilization does not increase with the control horizon within the MPC<sup>3</sup> framework. This enables autonomous applications which were deemed infeasible due to high computational cost and memory usage.

## IV. APPLICATION TO SPACE PROXIMITY OPERATIONS

The Transforming Proximity Operations and Docking System (TPODS) is a conceptual 1U CubeSat module, developed by the Land, Air and Space Robotics (LASR) laboratory at Texas A&M University [31], [32], [33]. The proposed MPC<sup>3</sup> framework is utilized to enable robust and safe proximity operations of the TPODS module. The objective is to dock a chaser TPODS to a stationary target using a multi-state guidance algorithm. The TPODS module is equipped with Ultra-Wide-Band (UWB) radar range and monocular-vision camera sensors [33]. A unified pose estimator can be leveraged to fuse the range from stationary anchors with monocular vision data to produce consistent pose estimates [34]. The guidance logic for the docking scenarios considered in this paper is shown in Fig. 1.

<sup>1</sup><https://www.pjrc.com/store/teensy41.html>

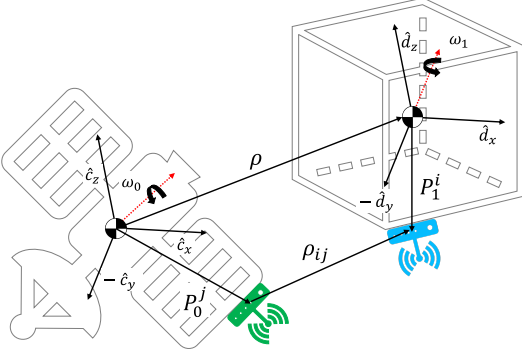


Fig. 5. Arrangement of UWB transceiver on TPODS module and stationary anchors. Since the anchors and UWB sensor are not mounted at respective centers of mass, the rotational and translation motion of the UWB sensor relative to the stationary anchors are coupled.

### A. System Dynamics

From the arrangement shown in Fig. 5, the motion governing equations for the chaser TPODS are [33]

$$\ddot{\rho}_{ij} = \ddot{\rho} + \dot{\omega} \times P_1^i + \omega \times (\omega \times P_1^i) \quad (43)$$

$$I_0 \dot{\omega} = I_0 D (I_1)^{-1} [N_1 - D^T \omega \times I_1 D^T \omega] \quad (44)$$

Here,  $D$  is the rotation matrix that transforms vectors from TPODS reference frame  $\hat{d}$  to the mother-ship frame  $\hat{e}$ ,  $\omega$  is the rotational angular velocity of TPODS relative to the mother-ship,  $I_0$  and  $I_1$  are respective inertia tensors for the mother-ship and TPODS and  $N_1$  is the external torque applied to the TPODS. The CubeSat module has ten nozzles arranged in an ‘X’ configuration on each opposite face to enable 6-DOF [33].

For the simulation studies presented in this section, the linearized dynamics of the double-integrator in three translation axes are considered for the constrained optimization problem. Once the set of optimal control inputs is obtained for the selected control horizon, the control inputs at the first instance are determined and applied to the non-linear dynamics given by Eqs. (43) and (44), and the true states are propagated. The current states are fed to the multi-state guidance algorithm after an appropriate process noise has been injected into the velocity states. Finally, the desired values of the attitude and position computed by the guidance algorithm are fed to the optimization routine and the process continues.

### B. Keep-Out-Constraint

One of the prominent safety requirements for the majority of real-world operations is Keep-Out-Constraints (KOC). Due to inherent uncertainties associated with localizing objects, it is necessary to account for the margin of safety. One of the ways this can be achieved is by prohibiting the presence of a chaser within a certain spherical or ellipsoidal volume. A few approaches to incorporate KOC in the MPC framework have been considered: a discontinuous augmented state [35], a repulsive pseudo-potential and differentiable

collision detection of polytopic convex hulls [36]. While using the augmented state, the violation has to occur once for KOC to be effective. This limitation results in a steep correction and a large force demand and is not desirable as it causes intense structural stress and increased fuel consumption.

An alternative to the discontinuous augmented state is smooth pseudo potential which repulses the chaser when near to the target. This repulsive pseudo potential can be in the form  $ar^{-l}$ , where  $r$  is the distance between the target and chaser. The tuning parameters  $a, l > 0$  depict the intensity of the repulsive action. These parameters, along with the cost weight factor, can be adjusted to get the desired radius of the KOC. One such example trajectory for  $a = l = 1$  is shown in Fig. 6. It is evident that the overall trajectory is considerably smoother and does not violate the KOC at all. It also achieves substantial fuel savings compared to the discontinuous augmented state.

Although the KOC with repulsive potential works well for symmetric bodies, it does not result in an efficient utilization of the feasible space for axisymmetric elongated bodies. For such scenarios, differential collision detection for convex polytopes (DCOL) can provide a robust and efficient avenue to enforce KOC [36]. Collision detection via DCOL works by inflating polytopic convex hulls of the target and chaser by a scaling factor  $s$ . When  $s$  is found to be greater than one, both bodies are separated. For a given set of polytopes, the minimum value of  $s$  can be computed by solving a linear program with inequality constraints stemming from the fact that the intersection point is a member of both inflated polytopes.

Once the collision is detected, corrective action needs to be taken such that the chaser moves away from the target. For the analysis presented in this paper, the target is considered

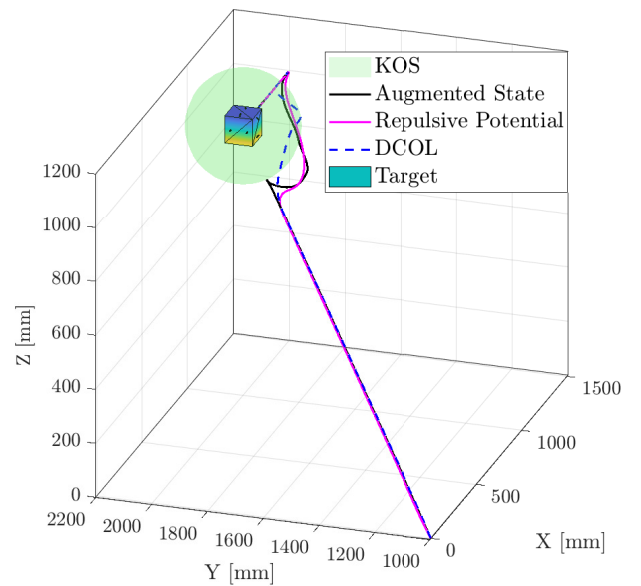


Fig. 6. Comparison of KOS constraint using discontinuous state, repulsive potential and differential polytopic hull.

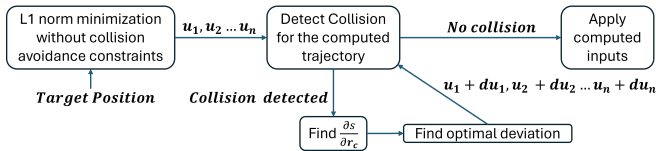


Fig. 7. Collision avoidance algorithm using differential collision detection of polytopic primitives

stationary and the attitude of the chaser is not varied during collision avoidance maneuvers. Hence, the general direction in which the separation is achieved can be inferred from the relative change of the  $s$  with respect to the position of the chaser. For the MPC framework, collision avoidance can be achieved with the process shown in Fig. 7 [37]. The optimization problem given by Eq. (34) is first solved without any additional collision avoidance constraints. Next, the value of  $s$  for all instances within the control horizon is computed.

If the value of  $s$  for any instance within the control horizon is less than a predefined soft limit  $s_{\text{thr}}$ , the partial derivative  $\frac{\partial s}{\partial \mathbf{r}_c}$  is computed and the optimization problem is modified as

$$\min_{\mathbf{u}, d\mathbf{u}, \epsilon} \quad \|\mathbf{u} + d\mathbf{u}\|_2 + \|\mathbf{y} - \mathbf{y}_{\text{tar}}\|_2 + \rho\epsilon^2 \quad (45)$$

$$\text{s.t.} \quad \dot{\mathbf{x}} = \mathbf{A}\mathbf{x} + \mathbf{B}(\mathbf{u} + d\mathbf{u}) \quad (46)$$

$$\mathbf{u}_{\text{max}} \geq |\mathbf{u} + d\mathbf{u}| \quad (47)$$

$$s_{\text{thr}} \leq s + \frac{\partial s}{\partial \mathbf{r}_c} \frac{\partial \mathbf{r}_c}{\partial (\mathbf{u} + d\mathbf{u})} + \rho\epsilon \quad (48)$$

The modified input sequence which ensures a collision-free trajectory is then applied to the chaser and the process is repeated until the chaser is within a specified radius of the target. As shown in Fig. 6, collision avoidance with DCOL results in a smooth trajectory with the least deviation from the intended optimal trajectory among all approaches analyzed. In addition to the least energy consumption, the collision avoidance approach based on the polytopic hulls of respective bodies prevents the optimization problem from becoming infeasible due to geometrical complexities [36].

### C. Optimal Trajectories for Docking

To validate the proposed framework, the orientation of the docking face on the target and the initial pose of the chaser is selected such that the extremal trajectory of the chaser passes through the target. Individual translation velocities are restricted to 0.02 m/s with a softness factor of 0.1 and the control forces are restricted to 10 mN in each axis with a softness factor of 0.01. The soft target for scaling factor  $s_{\text{thr}}$  is picked as 1.5 to ensure robustness against pose estimation errors. The collision detection and avoidance is switched on when the chaser is within 0.4 m radius of the target and switched off during the final phase of docking. The attitude controller acts independently and leverages errors in desired and current quaternion to drive the chaser to the desired orientation during various guidance modes [34].

From the time histories of translation velocities presented in Fig. 8, the effectiveness of the soft constraints on the ve-

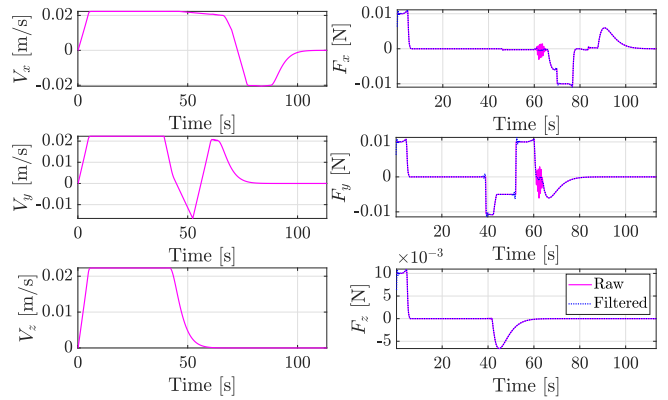


Fig. 8. Time history of translation velocities and desired forces for docking scenario shown in Fig. 1

locity can be observed. The algorithm successfully manages to restrict the velocities around the enforced soft limits. As mentioned earlier, these constraints can be enforced more aggressively using respective softness parameters and their violations can be heavily penalized using the weight factor of the slack variable.

Barring the sporadic chattering, the desired forces also remain within the specified constraints throughout the motion. The isolated oscillations increase but average out towards the true discontinuous control with approximation order and are more generally known as Gibbs phenomenon [21]. These are undesirable and can result in wear and tear of the actuators. However, a careful selection of the weight factors and intermediate band-reject filters can help eliminate the oscillations to produce smooth control commands.

Finally, to assess the robustness of the collision avoidance algorithm, 500 run Monte Carlo simulations are performed. The true states of the chaser are infused with an appropriate process noise while the target position and initial position of the chaser are left unchanged. The trajectory of the scaling factor for all Monte Carlo iterations is shown in Fig. 9, where the effectiveness of the collision avoidance algorithm in keeping the scaling factor near the soft threshold is evident. The softness of translation velocity and collision avoidance constraints helps in keeping the optimization problem feasible, ensuring tractable input forces.

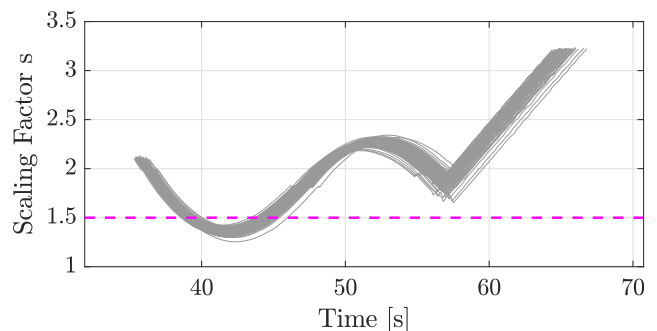


Fig. 9. Scaling factor for 500 run Monte Carlo simulations.

## V. CONCLUSIONS

A computationally efficient trajectory optimization and control framework using integral Chebyshev collocation is introduced in this paper and its performance is compared with existing optimization solvers, on a conventional and edge computers. The utility of the framework is demonstrated by formulating a model predictive controller to enable proximity operations of CubeSat agents. The state and control inequality constraints are added, along with functionality to define softness/hardness to enhance the practicality of the framework. A robust and efficient collision avoidance based on polytopic hulls makes this framework particularly attractive for the majority of the real-world applications. The current focus of the authors is to demonstrate the planar proximity operations of TPODS MK-E motion emulators using the MPC<sup>3</sup> framework and packaging for eventual release, enabling widespread adoption for resource constrained autonomous applications.

## ACKNOWLEDGEMENT

Program monitors for the AFOSR SURI on OSAM, Dr. Andrew Sinclair and Mr. Matthew Cleal of AFRL are gratefully acknowledged for their watchful guidance. Prof. Howie Choset of CMU, Mr. Andy Kwas of Northrop Grumman Space Systems and Prof. Rafael Fierro of UNM are acknowledged for their motivation, technical support, and discussions. Dr. Geordan Gutow of CMU is acknowledged for introducing DCOL framework the authors.

## REFERENCES

- [1] E. Rodgers, "The future of space operations," in *AIAA SciTech Forum and Exposition*, January 2024.
- [2] H. Sanchez, D. McIntosh, H. Cannon, C. Pires, J. Sullivan, S. D'Amico, and B. O'Connor, "Starling1: Swarm technology demonstration," 2018.
- [3] E. Adams, D. O'Shaughnessy, M. Reinhart, J. John, E. Congdon, D. Gallagher, E. Abel, J. Atchison, Z. Fletcher, M. Chen, et al., "Double asteroid redirection test: The earth strikes back," in *2019 IEEE Aerospace Conference*, pp. 1–11, IEEE, 2019.
- [4] N. T. Redd, "Bringing satellites back from the dead: Mission extension vehicles give defunct spacecraft a new lease on life-[news]," *IEEE Spectrum*, vol. 57, no. 8, pp. 6–7, 2020.
- [5] A. Ogilvie, J. Allport, M. Hannah, and J. Lymer, "Autonomous satellite servicing using the orbital express demonstration manipulator system," in *Proc. of the 9th International Symposium on Artificial Intelligence, Robotics and Automation in Space (i-SAIRAS'08)*, pp. 25–29, 2008.
- [6] G. Visentin and D. Brown, "Robotics for geostationary satellite servicing," *Robotics and Autonomous Systems*, vol. 23, no. 1, pp. 45–51, 1998. Space Robotics in Europe.
- [7] Z. Vafa and S. Dubowsky, "The kinematics and dynamics of space manipulators: The virtual manipulator approach," *The International Journal of Robotics Research*, vol. 9, no. 4, pp. 3–21, 1990.
- [8] M. Shibli, F. Aghili, and C.-Y. Su, "Modeling of a free-flying space robot manipulator in contact with a target satellite," in *Proceedings of 2005 IEEE Conference on Control Applications, 2005. CCA 2005.*, pp. 559–564, 2005.
- [9] B. F. Knight, "Advances in space trusted autonomy," in *Autonomous Systems: Sensors, Processing, and Security for Ground, Air, Sea, and Space Vehicles and Infrastructure 2024*, vol. 13052, p. 1305208, SPIE, 2024.
- [10] J. Rudico, J. T. Nichols, and G. Rogers, *Potential United States Space Force Mission Life Extension Applications*.
- [11] B. Yost and S. Weston, "State-of-the-art small spacecraft technology," tech. rep., National Aeronautics and Space Administration, 2024.
- [12] D. Selva and D. Krejci, "A survey and assessment of the capabilities of cubesats for earth observation," *Acta Astronautica*, vol. 74, pp. 50–68, 2012.
- [13] A. G. Guerra, F. Francisco, J. Villate, F. Aguado Agelet, O. Bertolami, and K. Rajan, "On small satellites for oceanography: A survey," *Acta Astronautica*, vol. 127, pp. 404–423, 2016.
- [14] H. E. Spence et al., "Achievements and lessons learned from successful small satellite missions for space weather-oriented research," *Space Weather*, vol. 20, no. 7, p. e2021SW003031, 2022. e2021SW003031 2021SW003031.
- [15] S. J. Qin and T. A. Badgwell, "An overview of industrial model predictive control technology," in *AIChE symposium series*, vol. 93, pp. 232–256, New York, NY: American Institute of Chemical Engineers, 1971-c2002., 1997.
- [16] U. Eren, A. Prach, B. B. Koçer, S. V. Raković, E. Kayacan, and B. Açıkmeşe, "Model predictive control in aerospace systems: Current state and opportunities," *Journal of Guidance, Control, and Dynamics*, vol. 40, no. 7, pp. 1541–1566, 2017.
- [17] K. Nguyen, S. Schoedel, A. Alavilli, B. Plancher, and Z. Manchester, "Tinympc: Model-predictive control on resource-constrained microcontrollers," in *IEEE International Conference on Robotics and Automation (ICRA)*, 2024.
- [18] A. Fear and E. G. Lightsey, "Autonomous rendezvous and docking implementation for small satellites using model predictive control," *Journal of Guidance, Control, and Dynamics*, vol. 47, no. 3, pp. 539–547, 2024.
- [19] J. T. Betts, "Survey of numerical methods for trajectory optimization," *Journal of guidance, control, and dynamics*, vol. 21, no. 2, pp. 193–207, 1998.
- [20] X. Bai, *Modified Chebyshev-Picard Iteration Methods for Solution of Initial Value and Boundary Value Problems*. PhD thesis, Texas A&M University, 2010.
- [21] C. Peck, *Adaptive Collocation Methods Using Chebyshev Integration*. PhD thesis, Texas A&M University, 2023.
- [22] L. Fox and I. B. Barker, *Chebyshev Polynomials in Numerical Analysis*. Oxford University Press, 1968.
- [23] X. Bai and J. L. Junkins, "Modified chebyshev-picard iteration methods for solution of boundary value problems," *Journal of Astronautical Sciences*, vol. 58, pp. 615–642, 2011.
- [24] J. P. Boyd, *Chebyshev and Fourier spectral methods*. Courier Corporation, 2001.
- [25] A. P. Prudnikov, Y. A. Brychkov, and O. I. Marichev, *Integrals and Series, Volume 2: Special Functions*. Gordon and Breach Science Publishers, 1986.
- [26] J. Rawlings, D. Mayne, and M. Diehl, *Model Predictive Control: Theory, Computation, and Design*. Nob Hill Publishing, 2017.
- [27] F. Borrelli, A. Bemporad, and M. Morari, *Predictive Control for Linear and Hybrid Systems*. Cambridge University Press, 2017.
- [28] C. F. Gauss, "Methodus nova integralium valores per approximationem inveniende," *Comment Soc. Reg. Scient. Gotting*, pp. 39–76, 1814.
- [29] S. E. Notaris, "Interpolary quadrature formulae with chebyshev abscissae," *Journal of Computational and Applied Mathematics*, vol. 133, pp. 507–517, 2001.
- [30] G. Banjac, B. Stellato, N. Moehle, P. Goulart, A. Bemporad, and S. Boyd, "Embedded code generation using the OSQP solver," in *IEEE Conference on Decision and Control (CDC)*, 2017.
- [31] D. Parikh et al., "A scalable tabletop satellite automation testbed: Design and experiments," in *2023 AAS - Rocky Mountain GN&C Conference*, 02 2023.
- [32] D. Parikh and M. Majji, "Estimation of inertial properties of a rigid structure maneuvered by satellite modules," in *2023 AAS/AIAA Astrodynamics Specialist Conference, Big Sky, Montana*, 08 2023.
- [33] D. Parikh and M. Majji, "Pose estimation of cubesats via sensor fusion and error-state extended kalman filter," in *2024 AAS - Rocky Mountain GN&C Conference*, 02 2024.
- [34] D. Parikh, A. H. Khawaja, and M. Majji, "Robust proximity operations using probabilistic markov models," in *IEEE International Conference on Robotics and Automation (ICRA)*, 2025 [Manuscript Submitted].
- [35] D. Parikh and A. Tewari, "Optimal landing strategy on a uniformly rotating homogeneous rectangular parallelepiped," *The Journal of the Astronautical Sciences*, vol. 68, 12 2020.
- [36] K. Tracy, T. A. Howell, and Z. Manchester, "Differentiable collision detection for a set of convex primitives," in *2023 IEEE International Conference on Robotics and Automation (ICRA)*, pp. 3663–3670, 2023.
- [37] I. S. Sow, G. Gutow, H. Choset, and Z. Manchester, "A convex formulation of the soft-capture problem," 2024.